Planetary and Space Science 73 (2012) 310–317

Contents lists available at SciVerse ScienceDirect

Planetary and Space Science

journal homepage: www.elsevier.com/locate/pss

First ever VLF monitoring of the lunar occultation of a solar flare during the 2010 annular solar eclipse and its effects on the D-region electron density profile

Sujay Pal [a,b,*], Surya K. Maji [b], Sandip K. Chakrabarti [a,b]

[a] S. N. Bose National Centre for Basic Sciences, JD Block, Sector-III, Salt Lake, Kolkata 700098, India
[b] Indian Centre for Space Physics, 43 Chalantika, Garia St. Road, Kolkata 700084, India

ARTICLE INFO

Article history:
Received 4 April 2012
Received in revised form
12 August 2012
Accepted 14 August 2012
Available online 24 August 2012

Keywords:
Solar eclipse
Solar flare
D-region
Ionosphere
VLF
Electron density
Occultation

ABSTRACT

A ground based Very Low Frequency (VLF) radio receiver of Indian Centre for Space Physics located at Khukurdaha (22°27′N, 87°45′E) monitored the VLF signal at 19.8 kHz from the NWC station during a partial solar eclipse (maximum obscuration 75%) which took place on January 15, 2010. The receiver and the transmitter were on two opposite sides of the annular eclipse belt. During the same period, a solar flare also occurred and it was partly blocked by the lunar disk. Thus the resultant signal was perturbed both by the eclipse and by the flare. The deviation of the signal from the normal value was obtained by subtracting from the average diurnal signal on days bracketing the eclipse. The deviation was analysed. We compare the data from GOES-14, HINODE and RHESSI satellites during the event. We got a clear depression in the data during the period of the partial eclipse. Most interestingly, there was also a flaring activity in the sun which reached its peak (C-type) just after the time when the eclipse was near maximum. By superposing the lunar disk on the image obtained by HINODE mission, we pinpoint the time frame of blocking hard and soft X-rays. We extract the time variation of the electron density profile in the D-region of the ionosphere due to occulted solar flare from the combined effect of the eclipse and the flare. We also compare the results with a normal solar flare.

1. Introduction

Very Low Frequency (VLF) radio waves are used for long distance communication for their very low attenuation while propagating through the Earth-ionosphere wave guide. Indian Centre for Space Physics has been monitoring VLF radio wave transmitting stations from several of its monitoring stations. On January 15, 2010, there was an annular solar eclipse as seen from the southern regions of India. At Khukurdaha (22°27′N, 87°45′E) station, the eclipse was partial with a maximum obscuration of about 75%. From this station, we have been monitoring NWC transmitter operating at 19.8 kHz. We report the results of our observations *and interpretations* in this paper.

Periodic variation of the solar radiation on the upper atmosphere each day due to sunrise and sunset gives rise to a periodical variation in its charge density. After the sunrise, the extreme ultraviolet and the soft X-ray radiations create the D-region lowering the ionospheric height to $\sim 60-70$ km. Solar eclipse has always been a very important calculable event which changes the ionosphere in a predictable time frame. During a partial eclipse, the ionosphere experiences a reduction in intensity of the UV and soft X-ray photons from the solar disk. This gives us an opportunity to study the global variation of electron concentration in the ionosphere which could be useful to understand the ion chemistry. Long wavelength propagation models inside the Earth-ionosphere wave guide may be tested as well.

The effects of the solar eclipse on the amplitude and phase of VLF signals over the both short (<3000 km) and long (>3000 km) propagation paths have been reported by many authors (Bracewell, 1952; Sen Gupta et al., 1980; Lynn, 1981; Buckmaster and Hansen, 1986; Mendes da Costa et al., 1995). Clilverd et al. (2001) reported the results of monitoring the VLF signals from multiple transmitters and receivers paths during the total solar eclipse of August 11, 1999 in Europe. They calculated the variation of electron density at 77 km altitude throughout the period of solar eclipse, which showed a linear variation in electron production rate with solar ionizing radiation. Pal et al. (2012) reported the effects of total solar eclipse of 2009 in India for several propagation paths and also modelled the VLF amplitude deviations due to the eclipse using the Long Wave Propagation Capability (LWPC) (Ferguson, 1998) code. Chakrabarti et al.

* Corresponding author at: Indian Centre for Space Physics, 43 Chalantika, Garia St. Road, Kolkata 700084, India. Tel.: +91 33 2335 5706/7/8x442; fax: +91 33 2335 3477.
E-mail address: sujay@bose.res.in (S. Pal).

0032-0633/$ - see front matter © 2012 Elsevier Ltd. All rights reserved.
http://dx.doi.org/10.1016/j.pss.2012.08.016

(2010, 2011a,b, 2012) presented results of observations during the Total Solar Eclipse (2009) from multiple receiving stations and found that for some stations, the amplitude of the signal is enhanced, while some other stations the amplitude is reduced from the normal values. Sudden ionospheric perturbations due to the solar flares are common (Mitra, 1974). The importance of our observation is that the flare and the eclipse both took place simultaneously and the effect of the flare is only partial due to the occultation by the moon.

In this paper, we describe our results in detail and compare the VLF signals with the light curve of hard and soft X-rays obtained by the GOES-14 and RHESSI satellites. We also present the magnetogram around the flare obtained by the GONG project and the image of the flare from the HINODE X-Ray Telescope (XRT) data. From the relative positions of the Sun, the Moon and the receiving station, we derive the time variation of the lunar occultation of the flare. From these, we obtain the time variation of the electron number density in the lower ionosphere over the entire event. In the next Section, we describe the events of which the results are reported. In Section 3, we present the experimental set-up, the process of data acquisition and the observational results, including those from various satellites. In Section 4, we separate the eclipse component and the flare component from the combined VLF signal. In Section 5, we simulate VLF signal received by us and derived ionospheric parameters, such as the electron number density and the reflection height. Finally in Section 6, we make concluding remarks.

2. The solar eclipse and the solar flare

The Indian Centre for Space Physics (ICSP) made Gyrator-III VLF receiver (1–22 kHz) with a loop antenna was monitoring NWC station from Khukurdaha. The annular solar eclipse of January 15, 2010 started at 12:05 IST (=UT+5:30) and continued up to 15:28 IST. The eclipse was partial (maximum coverage 75%) as seen from Khukurdaha. The maximum obscuration at the receiver occurred at 13:56:26 IST. The distance between transmitter and receiver is about 5700 km (Fig. 1). Thus the transmitter was far away from the annular solar eclipse belt. During propagation of signal from NWC to Khukurdaha, there was no eclipse in 24.5% of the total path while 75.4% of the total path experienced some eclipse. The whole propagation path experienced an average value of solar obscuration at the most 40% calculated using a numerical integration over the whole path. Fig. 2 shows the degree of solar obscuration during eclipse at receiver and over the whole path at 70 km above the ground.

While the eclipse is in process, a C1.3 solar flare started at 07:22 UT (12:52 IST) and continued till 10:22 UT (15:52 IST) with an extended maximum in Soft X-ray from 08:41 UT (14:11 IST) to 08:44 UT (14:14 IST) The hard X-ray peaked at 08:36 UT (14:06 IST). Thus the hard and the soft X-ray peak within the eclipse period. The soft X-ray peak is about 15 min after the maximum obscuration of the solar disk. The peak energy flux in 1.5–12.5 keV was 1.3×10^{-6} ergs/cm^2 which is well above the detectability limit of our VLF antenna (typically, C1.0 flare).

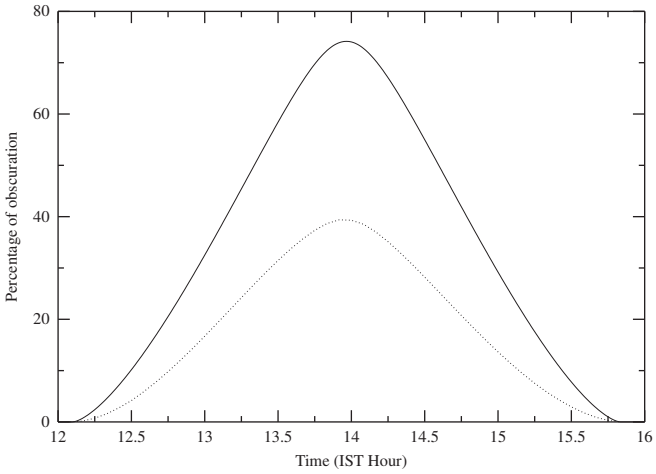

Fig. 2. Variation of percentage of solar obscuration (S) as a function of time. Solid curve represents the solar obscuration at the receiver and the dotted curve represents the average value of solar obscuration over the whole path.

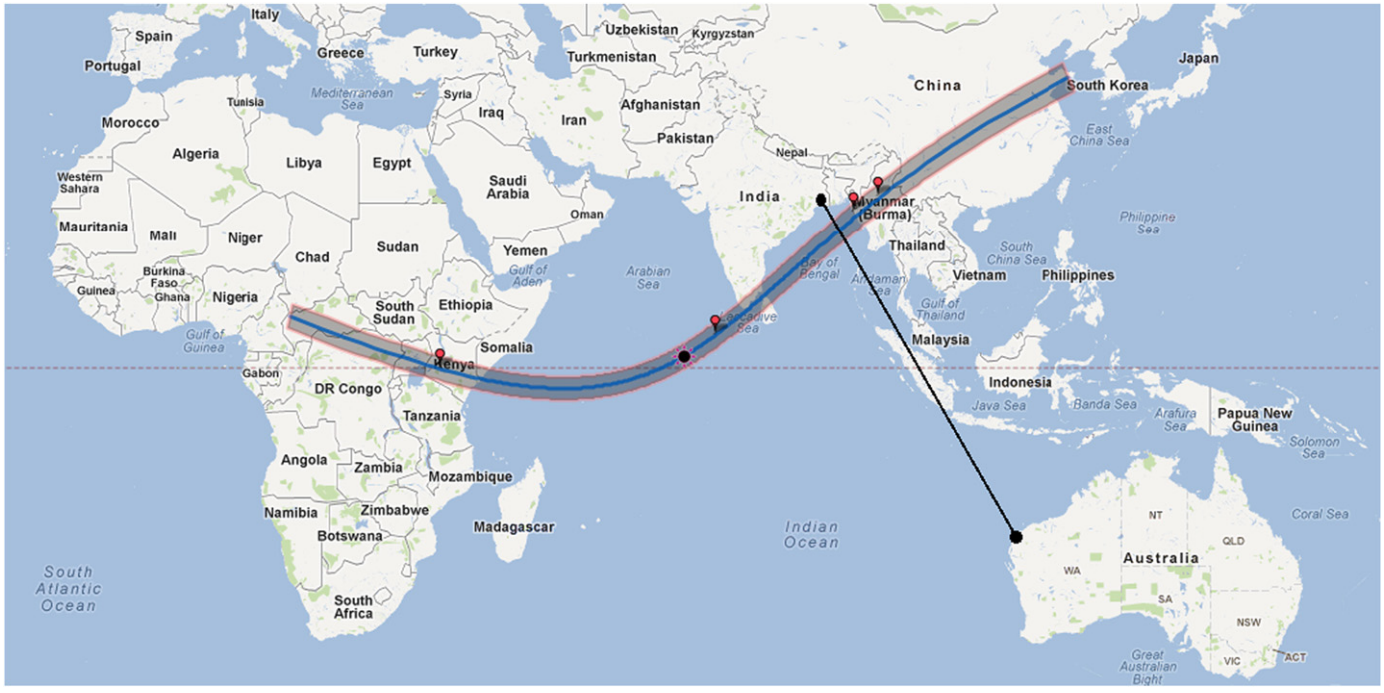

Fig. 1. Great circle path between the NWC transmitter and receiver. The shaded area is the path of total annularity of January 15, 2010.

3. The experimental set-up and the observational results

A loop antenna and Gyrator-III type receiver were deployed to monitor VLF data at Khukurdaha. Real time narrow band signal amplitudes from several transmitters were recorded automatically in the computer. In Fig. 3, we give an example of deviation of the NWC signal amplitude obtained from a C4.0 flare which occurred on February 6, 2010, three weeks after the solar eclipse event which we report here. For comparison with this, we also present the soft X-ray flux from the GOES-14 satellite of this flare.

In Fig. 4, we present the amplitude (dB) variation of the NWC signal as obtained by our receiver on January 15, 2010, the day of the annular eclipse. The box highlights the region around the eclipse which clearly shows a dip near the eclipse maximum and an upward rising kink near the flare maximum. The time is given in IST (=UT+5:30). In Fig. 5, we plotted the net deviation of NWC signal from the normal data which is defined as the average of the data of 14th and 16th January for the solar eclipse time only. Here, the upper panel shows the VLF amplitude deviation from the normal data due to the combined effect of solar eclipse and solar flare. Note that the net deviation due to the combined effect is 1.3 dB. In the middle panel, the dashed curve shows hard X-ray flux and the solid curve shows soft X-ray flux of the flare from GOES-14 satellite. The two vertical lines correspond to the time of maximum phase of the eclipse and the time at which the peak of the solar flare occurs. The lower panel shows the RHESSI data of X-ray flux in different energy bands for the same flare. Unfortunately, the satellite was over South Atlantic Anomaly region for much of the time (SAA) and the flare was seen only during the period denoted by F.

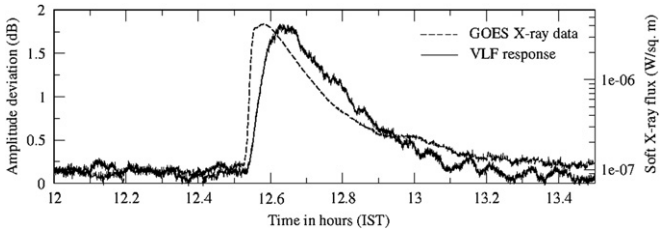

Fig. 3. Example of a normal (non-occulted) C4.0 solar flare which occurred on February 6, 2010. Dashed curve represents the GOES soft X-ray flux light curve and solid curve represents the NWC signal amplitude response to the flare.

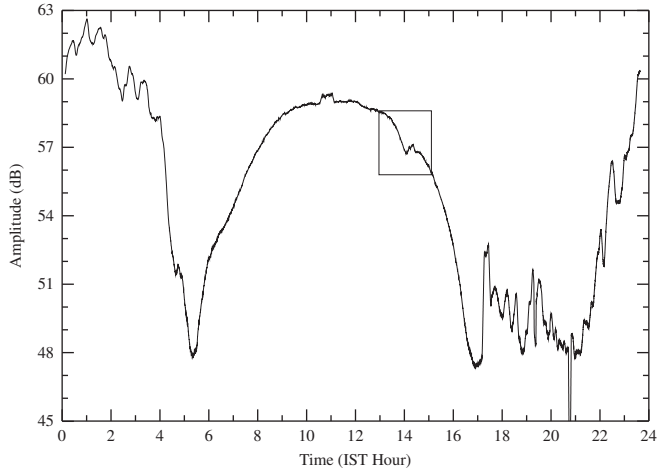

Fig. 4. The normalised diurnal variation of NWC signal on the eclipse day. The box highlights the ionospheric disturbances observed due to the joint effects of the eclipse and the flare. The time is in IST (UT+5:30).

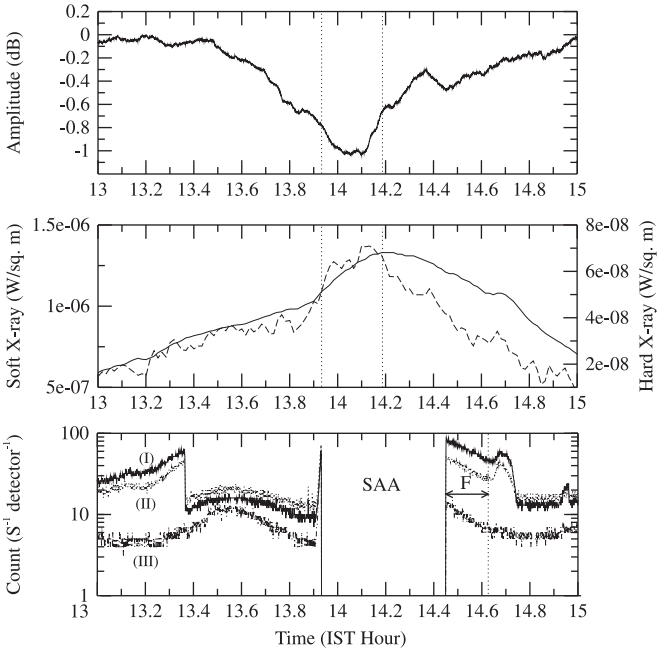

Fig. 5. Observed VLF data with GOES-14 and RHESSI soft and hard X-ray light curve. Upper panel shows the VLF amplitude deviation due to the combined effect of the solar eclipse and the solar flare obtained by subtracting the data of January 15th from the average of the normal data of 14th and 16th January, 2010. In the middle panel, the dashed curve shows the hard X-ray flux and solid curve shows the soft X-ray flux of the flare as obtained from the GOES satellite. Lower panel shows the RHESSI data of X-ray flux in different energy band at the same time. The region SAA and F marks the region over South Atlantic Anomaly and the period when the flare was observed by RHESSI. The curves marked by (I), (II) and (III) are for (3–6) keV, (6–12) keV and (12–25) keV respectively.

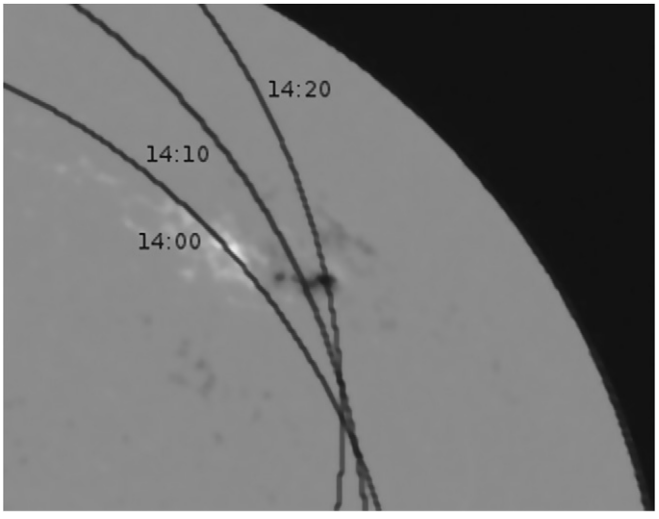

Fig. 6. Closer view of the positions of the lunar limb superimposed on the magnetogram (taken from GONG project data at 14:34 IST) of X-ray flaring region at different times to show that it was variously occulted by the moon from a direct view.

GOES satellite was observing the solar flare un-obstructed by the lunar occultation. In Fig. 6, we superimpose the position of the lunar limb on the magnetogram of the X-ray flaring region (AR 11040) at different times. This gives us an indication that the flare was partially occulted by the moon from the receiving station. In Fig. 7, the exposed solar disks are superimposed on the HINODE-XRT image of the solar flare during the solar eclipse at every 5 min, starting from 13:50:00 IST to 14:25:00 IST (top-left

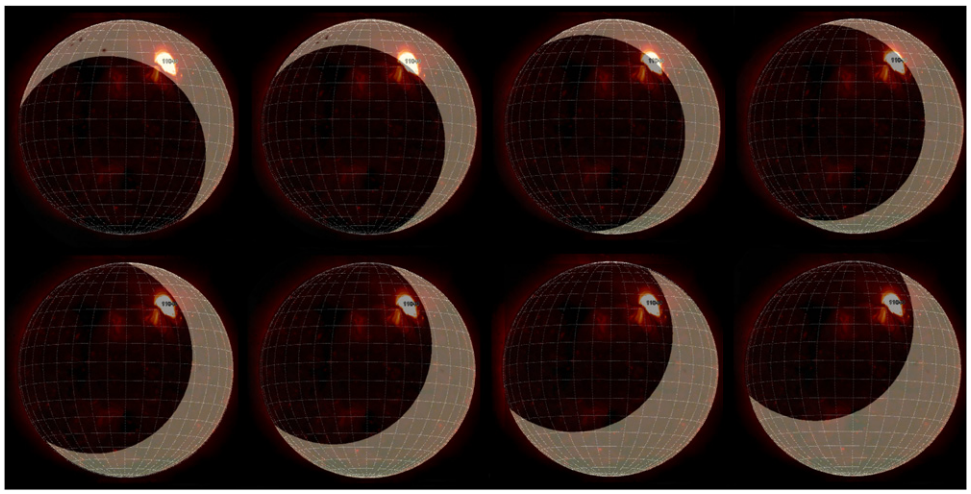

Fig. 7. Exposed solar disks at every 5 min (from top-left to top-right; bottom-left to bottom-right), starting from 13:50:00 IST to 14:25:00 IST, are superimposed on the XRT image of the solar flare during the solar eclipse.

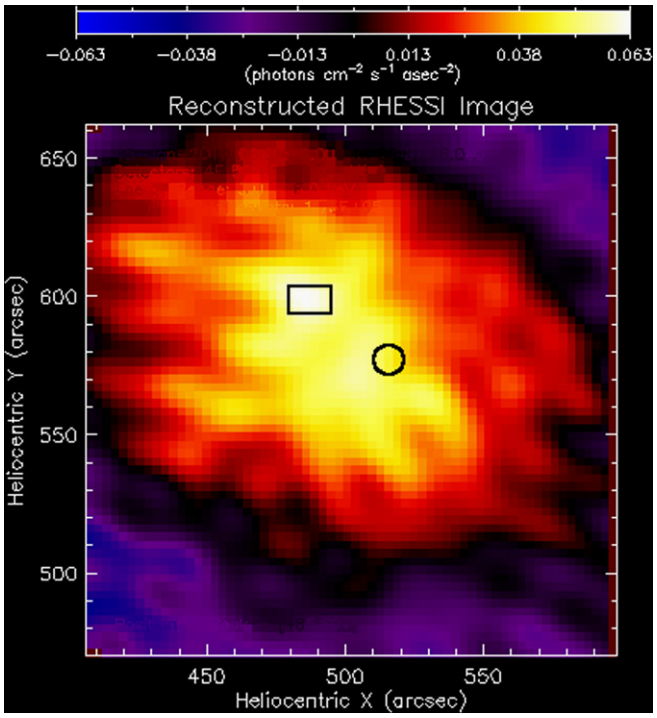

Fig. 8. In this RHESSI image, the black rectangle and circle show the peaks of soft X-ray (3–12 keV) and hard X-ray (12–25 keV) emitting regions. At 14:10 h (IST), the soft X-ray peak and between 14:20 and 14:25 h hard X-ray peak were covered by the moon.

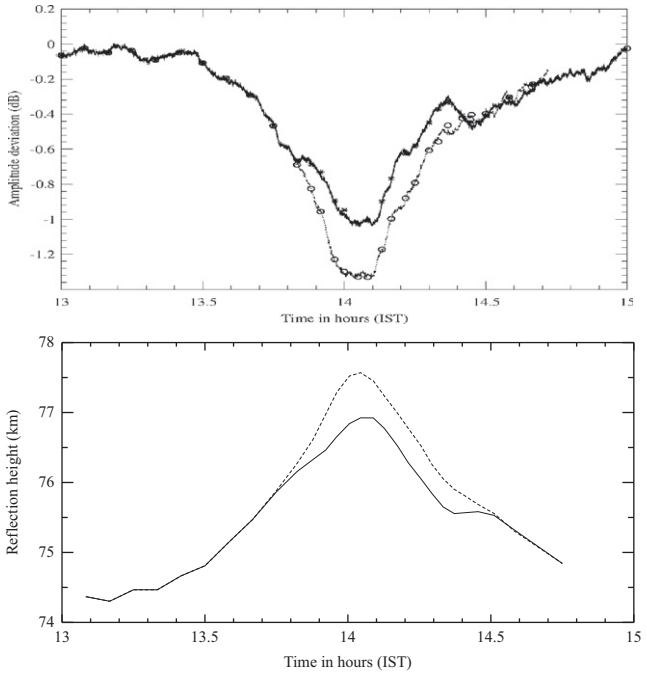

Fig. 9. (Top panel, a) Variation of differential amplitude of NWC (19.8 kHz) signal with time. The solid curve is the observed signal due to the combined effect of solar eclipse and the occulted X-ray flare. Dotted curve is the model signal if the flare were absent. Open circle and asterisk represent the times used for modeling electron density with LWPC. (Bottom panel, b) The corresponding effective reflection height variation.

to top-right; bottom-left to bottom-right). This shows that the flare is actually blocked by the moon.

In Fig. 8, we present the RHESSI image taken in the period marked by F in Fig. 5. Thus the image was taken just after the flare had the peak emission. However, assuming that the flare peak did not shift, we could identify the region where the peak emissions occurred. The black rectangular and circular regions show the peaks of the soft X-ray (3–12 keV) and hard X-ray (12–25 keV) emitting regions respectively. We find that the peak region of the soft X-ray was fully covered by the moon at 14:10 h (IST) and the hard X-ray peak region was covered from 14:20 to 14:25 h. It is interesting to note that the HINODE satellite also observed the occultation of the same flare but at a slightly different time and from a different perspective.

4. Separation of the effect of solar eclipse and that of the flare

Separation of the effects of the eclipse and the flare is tricky, since the flare is occulted partially by the moon during the eclipse. Thus, the observed VLF signal is neither due to the effect of the eclipse alone nor due to the flare alone. It is a composite effect that we observed. However, since the same antenna/receiver system has taken data from a similar flare at a similar time frame, we can separate the effects easily provided we assume that the effect is a linear superposition of the two effects. From Fig. 2 we obtain the nature of the VLF flare from a given C4.0 flare from the GOES data. We use this to obtain the possible signal that we would have obtained in case the eclipse was absent. This could have been subtracted from the observed VLF signal on

January 15, 2010, to obtain the possible signal due to eclipse, if the flare was absent. But in reality, only a part of the flare was absent as seen in Figs. 6 and 7. So we successively block the observed fraction of the flare using computed eclipse of the flare region and then subtract the effect. In Fig. 9a, we present two curves—the upper one is the deviation of the signal due to the combined effects. This is what we actually observe. The lower curve is obtained by subtracting the best estimated blocking of the flare by superposing the satellite images of the flaring region and the lunar disk. This would have been the signal deviation in case the flare was totally absent. This separation is thus due to the enhancement of the signal by the occulted flare. The open circles and the asterisks are the times when the LWPC code was used to obtain the electron number densities presented in the next Section. In Fig. 9b, we derive the variation of the effective height of the reflection level as obtained by the LWPC code. As expected, the reflection height would have been higher if the flare was absent (dashed curve). The presence of the flare lowers the height, but not as would have happened had its obscuration been absent.

5. Modeling VLF data and derivation of ionospheric parameters

Armed with the VLF signals with and without the flare, we can now model the time variation of the Earth's ionosphere. We use the Long Wavelength Propagation Capability (LWPC) (Ferguson, 1998) to calculate the amplitudes at receiving sites corresponding to normal and partially eclipsed-ionosphere conditions. LWPC code is very well known and it uses the waveguide mode theory. User of this model has to provide suitable lower and upper boundary conditions for the waveguide. The lower waveguide parameters i.e., permittivity (ϵ) and conductivity (σ) of the Earth have been automatically selected by the code itself. These parameters are constants corresponding to normal and eclipse conditions. The upper waveguide i.e., ionospheric parameters are specified by the electron density $N_e(h)$ and the electron-neutral collision frequency $v_e(h)$ profiles. We use Wait's exponential ionosphere (Wait and Spies, 1964) for electron density profile with gradient parameter β and reference height h' as given by the equation,

$$N_e(h,h',\beta) = 1.43 \times 10^7 \exp(0.15h')\exp[(\beta - 0.15)(h - h')]$$

in cm^3. The electron-neutral collision frequency (S^{-1}) is given by the equation,

$$v_e(h) = 1.816 \times 10^{11} \exp(-0.15h).$$

These profiles are very much well-known and generally agree with directly observed normal D-region ionospheric profiles (Sechrist, 1974; Cummer et al., 1998).

We took $h' = 71.0$ km and $\beta = 0.43$ km^{-1} as the unperturbed ionosphere (Thomson, 1993) while simulating the C4.0 flare, since these parameters reproduce the signal amplitude at receiver exactly as we observe. To model the partially eclipsed D-region ionosphere we need to calculate the degree of solar obscuration as a function of time along the path. For this we developed a numerical code to obtain the solar obscuration function $S(t)$ at a particular point along a path using the formalism of Mollmann and Vollmer (2006). The input parameters (i.e., the time of starting and ending of the eclipse, magnitude of eclipse) for the model are taken from the website of solar eclipse calculator (http://www.chris.obyrne.com/Eclipses/calculator.html) for the solar eclipse of January 15, 2010. We then divide the propagation path into several segments (~ 40) along the great circle path connecting the transmitter and the receiver. We calculate the degree of solar obscuration as a function of time. We find that $\sim 70\%$ of the total propagation path experienced partial solar eclipse.

The ionospheric responses to the incoming solar radiation are generally non-linear in the lower ionosphere (Lynn, 1981; Patel et al., 1986). To model the observed non-linearity between the solar illumination ($S(t)$) and VLF amplitude response, we assumed that the disturbed ionospheric parameters vary according to S^n, where S is the solar obscuration function on the points along the path. For this propagation path, comparing with our calculated effect of the solar eclipse, we found that the values of n lie between 1.5 and 1.0 from the start of the observed deviation to the maximum deviation.

We first apply this method to compute the time variation of enhanced electron number density due to a C4.0 flare (Fig. 3). Fig. 10 shows the plot. The colour scale shows the logarithmic

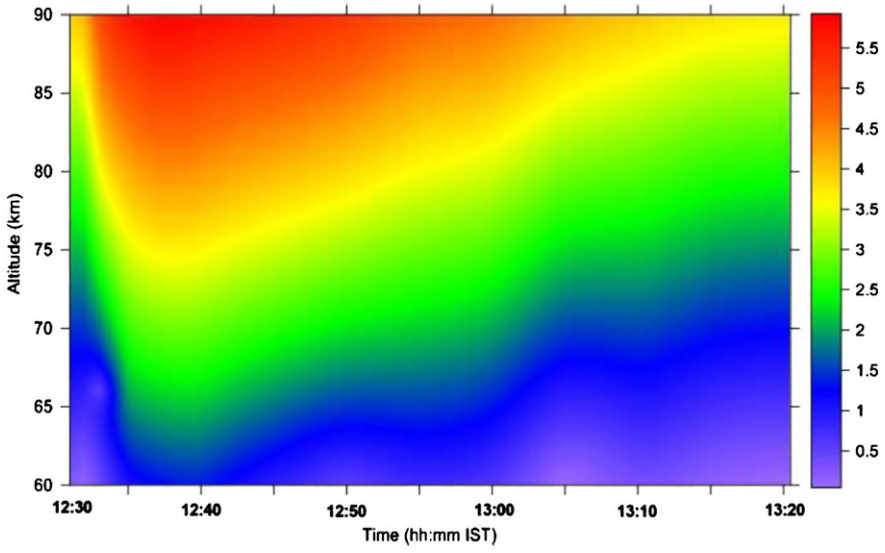

Fig. 10. Variation of electron number density (cm^{-3}) with altitude due to a normal C4.0 flare. The lower ionosphere decreases from 71 km to 68 km while the sharpness factor increases from 0.43 km^{-1} to 0.48 km^{-1}.

number density on the right. The numbers are comparable with that reported by Grubor et al. (2008). We found that the lower ionosphere came down from 71 km to 68 km, a decrease of 3.0 km, while the sharpness factor β increases from 0.43 km^{-1} to 0.48 km^{-1}.

We now apply the same method to compute how the electron number density changed in the ionosphere on January 15, 2010. Here, we choose $h' = 74$ km, and $\beta = 0.3$ km^{-1} as parameters for the unperturbed ionosphere (see, Fig. 9b). In Fig. 11, we show the results in presence of the eclipse and the occulted flare (top panel). The data was obtained by using LWPC at 'open circles' in the dotted curve of Fig. 9a. If we subtract the effects of the occulted flare as a function of time, and use the asterisks on the solid curve in Fig. 9a we get the electron density distribution as shown in Fig. 11b. In Fig. 12a, we show the difference of the number densities in the top and the bottom panels of Fig. 11. Far from having a profile similar to that in Fig. 10, we find a prominent dip in the electron number density at around 14:07 IST at all the altitudes. If we take cross-sections at different heights we get the time evolution of the electron number density of the ionosphere as a function of the height. We plot this in Fig. 12b. We find that below $\sim$60 km, the ionosphere is not perturbed significantly. With an increasing in height, there is a prominent dip in the middle. In fact, at 14:07 IST, the h' parameter is decreased by 0.41 km. This dip is due to the occultation of the flare. It appears that the soft X-ray peak is covered by 14:10 and the hard X-ray peak region is covered by 14:25 IST. The number density rises again when the flare is exposed again though the short-lived flare was already in its decaying phase by that time.

6. Concluding remarks

In this paper, we report and analysed a historic event, namely, the lunar occultation of a solar flare during an annular eclipse. This is the first time VLF monitoring was carried out during the event, and the VLF signal contains the effects of the all the three events, namely, the solar flare, lunar occultation of it and the eclipse itself. Although a flare was observed during a lunar occultation before (Kreplin and Taylor, 1971), there was no VLF monitoring of that event. We used the data from a multiple number of satellite and ground based observations, such as the GOES-14 (both hard and soft X-Ray light curves), GONG Project

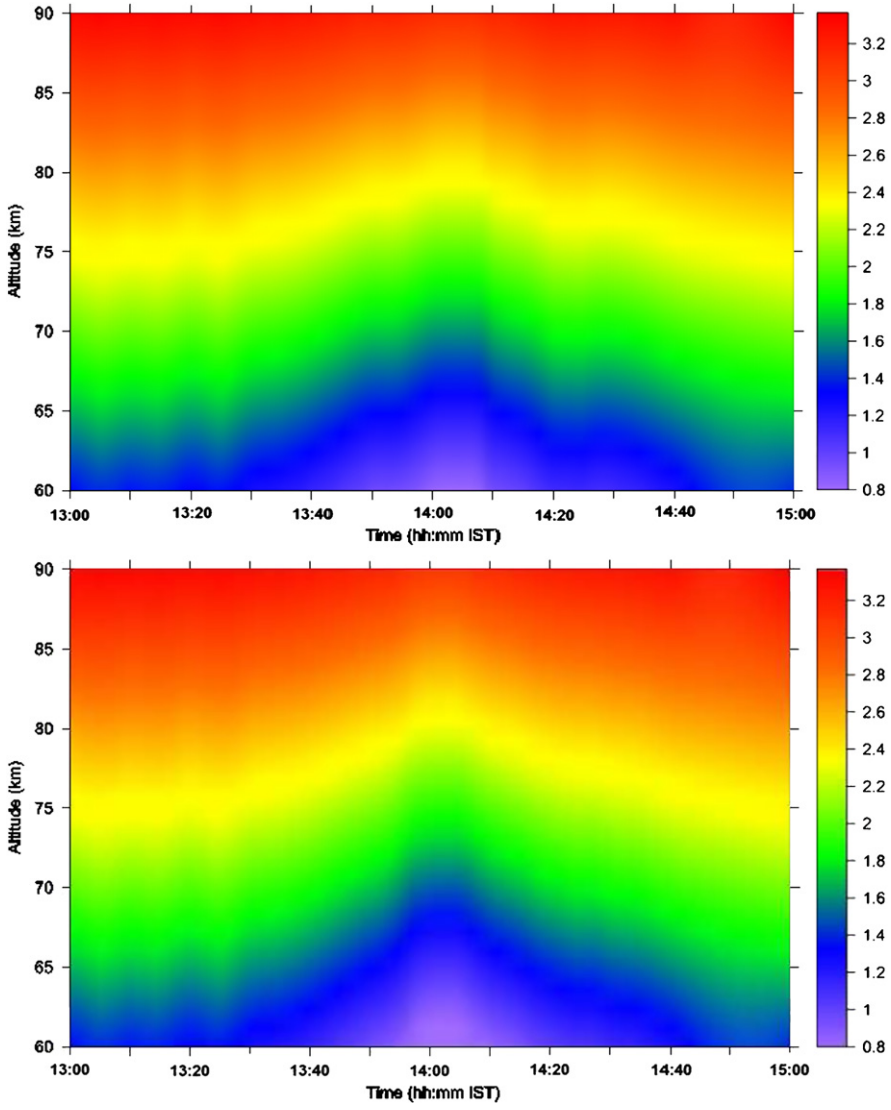

Fig. 11. Variation of electron density in logarithmic scale (cm^{-3}) with altitude for the combined effects (top panel, a) (solid curve in Fig. 9a) and (bottom panel, b) for the eclipse effect only (dashed curve in Fig. 9a).

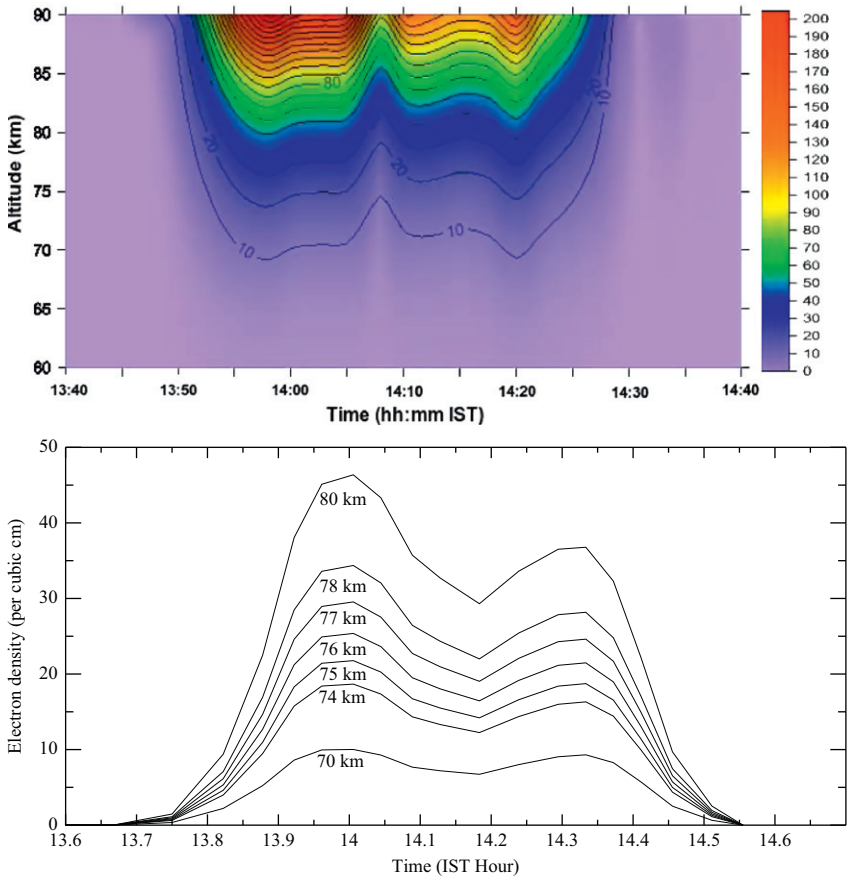

Fig. 12. (Top panel, a) The electron number density variation induced only by the flare and occultation (difference between Fig. 11a and Fig. 11b) in linear scale. The dip between 14:05 and 14:10 is consistent with the obscuration of the soft X-ray peak (see, Figs. 6–8). (Bottom panel, b) Variation of electron density (cm^{-3}) at different layers of the ionosphere at receiver location due to the occulted X-ray flare.

(Magnetogram data), HINODE (images of the flare) RHESSI (for X-ray light curves and image) which in conjunction with the VLF signal gives a time line of the sequence of events which took place. We find that because the eclipse was partial from our monitoring site, the flare was not totally occulted. This allows our pinpointing exactly when the soft and hard X-ray emitting peaks were occulted. Using our time-line of the event, which was independently verified by the magnetogram and HINODE/RHESSI images, we have been able to reproduce the possible VLF signal for the effects of the partial eclipse only. We accordingly computed the electron density profile of the eclipsed ionosphere. We also computed the enhanced electron number density solely due to the occulted flare and clearly found the effects of the occultations of the soft and hard peak emission regions. The eclipse causes the effective reflection height to rise as the electron number density decreases. On the other hand, the effect of the solar flare, which is present throughout the eclipse period, is to partially counteract the eclipse behaviour by increasing the electron density and decreasing the reflection height. The radiation from the solar flare and its ionospheric effect is briefly interrupted when the flare is occulted by the moon.

Acknowledgements

The authors acknowledge http://sec.noaa.gov for GOES data, http://hesperia.gsfc.nasa.gov for RHESSI data, http://www.solarmonitor.org for HINODE data and http://gong.nso.edu for GONG project data. SP acknowledges the support from a CSIR NET scholarship and SKC and SM acknowledge the support of a RESPOND project.

References

Bracewell, R.N., 1952. Theory of formation of an ionospheric layer below E layer based on eclipse and solar flare effects at 16 kc/s. Journal of Atmospheric and Terrestrial Physics 2, 226–235.
Buckmaster, H.A., Hansen, C.H., 1986. 26 February 1979 total solar eclipse induced LF (60 kHz) phase retardation. Journal of Atmospheric and Terrestrial Physics 48, 393–397.
Chakrabarti, S.K., Sasmal, S., Pal, S., Mondal, S.K., 2010. Results of VLF campaigns in summer, winter and during solar eclipse in Indian subcontinent and beyond. In: AIP Conference Proceedings, vol. 1286, AIP, New York.
Chakrabarti, S.K., Pal, S., Sasmal, S. et al., 2011a. VLF observational results of total eclipse of 22nd July, 2009 by ICSP team. IEEE Conference Publication, http://dx.doi.org/10.1109/URSIGASS.2011.6051005.
Chakrabarti, S.K., Mondal, S.K., Sasmal, S., et al., 2011b. VLF signals in summer and winter in the Indian sub-continent using multi-station campaigns. Indian Journal of Physics 86 (5), 323–334, http://dx.doi.org/10.1007/s12648-012-0070-x.
Chakrabarti, S.K., Pal. S., Sasmal. S., et al., 2012. VLF campaign during the total eclipse of July 22nd, 2009: observational results and interpretations. Journal of Atmospheric and Solar-Terrestrial Physics 86, 65–70. http://dx.doi.org/10.1016/j.jastp.2012.06.006.
Clilverd, M.A., Rodger, C.J., Thomson, N.R., et al., 2001. Total Solar Eclipse effects on VLF signals: observations and modeling. Radio Science 36 (4), 773.
Cummer, S.A., Inan, U.S., Bell, T.F., 1998. Ionospheric D region remote sensing using VLF radio atmospherics. Radio Science 33, 1781–1792.
Ferguson, J.A., 1998. Computer Programs for Assessment of Long-Wavelength Radio Communications, version 2.0. Technical document 3030, Space and Naval Warfare Systems Center, San Diego.
Grubor, D.P., Sulic, D.M., Zigman, V., 2008. Annals of Geophysics 26, 1731.
Kreplin, R.W., Taylor, R.G., 1971. Localization of the source of flare X-ray emission during the eclipse of 7 March, 1970. Solar Physics 21, 452.
Lynn, K.J.W., 1981. The total solar eclipse of 23 October, 1976 observed at VLF. Journal of Atmospheric and Terrestrial Physics 43, 1309–1316.
Mendes da Costa, A., Paes Leme, N.M., Rizzo Piazza, L., 1995. Lower ionosphere effect observed during the 30 June 1992 total solar eclipse. Journal of Atmospheric and Terrestrial Physics 57, 13–17.
Mitra, A.P., 1974. Ionospheric Effects of Solar Flares, vol. 46. D. Reidel, Norwell, MA, p. 307.

Mollmann, K.P., Vollmer, M., 2006. Measurements and predictions of the illuminance during a solar eclipse, 2006. European Journal of Physics 27, 1299.
Pal, S., Chakrabarti, S.K., Mondal, S.K., 2012. Modeling of sub-ionospheric VLF signal perturbations associated with total solar eclipse, 2009 in Indian subcontinent. Advances in Space Research 50, 196–204.
Patel, D.B., Kotadia, K.M., Lele, P.D., Jani, K.G., 1986. Absorption of radio waves during a solar eclipse. Earth and Planetary Science 95, 193–200.
Sechrist Jr., C.F., 1974. Comparisons of techniques for measurement of D-region electron densities. Radio Science 9, 137–149.
Sen Gupta, A., Goel, G.K., Mathur, B.S., 1980. Effect of the 16 February 1980 solar eclipse on VLF propagation. Journal of Atmospheric and Terrestrial Physics 42, 907.
Thomson, N.R., 1993. Experimental daytime VLF ionospheric parameters. Journal of Atmospheric and Terrestrial Physics 55, 173–184.
Wait, J.R., Spies, K.P., 1964. Characteristics of the Earth-Ionosphere Waveguide for VLF Radio Waves. NBS Technical Note, US 300.